Online Supplement:

Hernández et al. "Density dependence impacts our understanding of population resilience,"

The American Naturalist

Christina M. Hernández[1,*]

Iain Stott[2]

David Koons[3]

Roberto Salguero-Gómez[1]

1. Department of Biology, University of Oxford, Oxford, UK;

2. School of Natural Sciences, University of Lincoln, Lincoln, UK;

3. Department of Fish, Wildlife, and Conservation Biology, Colorado State University, Fort Collins, Colorado, USA.

∗ Corresponding author; e-mail: cmhernan@odu.edu

S1 Density dependence in demographic parameters

For survival, progression, and reproductive output, we used an exponential form of negative density dependence (Eq. S1). The general form is

$$\alpha(N) = \alpha_{max} e^{-bN}, \tag{S1}$$

where α_{max} is the maximum value that a given vital rate can take, and $\alpha(N)$ is that vital rate's value at a given value of population density ($N = n_a + n_j$). For all analyses in this paper, we use $b = 1$, indicating that all vital rates respond to density-dependence with the same strength.

The only vital rate that did not follow this functional form in our model framework was retrogression (ρ). Instead, we sought a functional form where the probability of retrogression would increase with higher population density. We selected a saturating functional form, where retrogression probability is 0 at very low densities ($N \approx 0$) and increases up to a selected maximum value (asymptotically):

$$\rho(N) = \rho_{max} \ln(N + 1) \tag{S2}$$

To ensure that $\rho(1)$ would have a pre-determined value, we set ρ_{max} to $\frac{\rho(1)}{\ln 2}$. This value is the result of re-arranging Equation S1 to solve for ρ_{max}.

S2 Model tuning for density dependence

To compare the response to population density across a wide range of life history strategies, we re-scaled our models to a carrying capacity of 1, enabling us to examine the resilience of all life history strategies across the same range of population density values, from $N = 0$ to $N = 1$.

For each density-dependent vital rate scenario, we solved analytically for per-capita reproductive output (ϕ) or maximum per-capita reproductive output (ϕ_{max}) value that corresponds to the population model having its equilibrium population size ('carrying capacity') at a density of 1.

Density is calculated as a simple sum of the number of juveniles and adults ($N(t) = n_j(t) + n_a(t)$).

The method for solving for ϕ or ϕ_{max} is as follows:

1. Write the population projection matrix with one vital rate as a function of density, following the form $\alpha(N) = \alpha_{max}e^{-bN}$.

2. Set this equation to its equilibrium population distribution for juveniles $\hat{n}_j$ and adults $\hat{n}_a$ such that these values are unchanged by projection to the next time step:

$$\hat{\mathbf{n}} = \mathbf{A}(\hat{\mathbf{n}}) \times \hat{\mathbf{n}}. \tag{S3}$$

3. Set $\hat{n}_j + \hat{n}_a = 1$.

4. Solve the resulting system of equations for ϕ (or ϕ_{max} in the scenario where ϕ is the density-dependent vital rate).

For example, in the case of density-dependent adult survival, we solve the system of equations, given in Eqs. S4 and S5, for ϕ.

$$\begin{bmatrix} \hat{n}_j \\ \hat{n}_a \end{bmatrix} = \begin{bmatrix} \sigma_j(1-\gamma) & \phi + \left(\sigma_{a,max}e^{-b(\hat{n}_j+\hat{n}_a)}\right)\rho \\ \sigma_j\gamma & \left(\sigma_{a,max}e^{-b(\hat{n}_j+\hat{n}_a)}\right)(1-\rho) \end{bmatrix} \times \begin{bmatrix} \hat{n}_j \\ \hat{n}_a \end{bmatrix} \tag{S4}$$

$$\hat{n}_j + \hat{n}_a = 1 \tag{S5}$$

The analytical solutions are as follows:

Density-dependent juvenile survival.

$$\phi = \frac{\left[1-(1-\gamma)\sigma_{j,max}e^{-b}\right]\left[(1-\gamma)-\sigma_a(1-\rho)(1-\gamma)\right]}{\gamma(1-\gamma)\sigma_{j,max}e^{-b}} - \sigma_a\rho \tag{S6}$$

Density-dependent progression.

$$\phi = \frac{-1}{\sigma_j \gamma_{max} e^{-b}} \left[\sigma_a \rho (\sigma_j - 1) + (\sigma_a - 1) \left(1 - \sigma_j (1 - \gamma_{max} e^{-b}) \right) \right] \tag{S7}$$

Density-dependent adult survival.

$$\phi = \frac{1 - \sigma_j (1 - \gamma) - \sigma_{a,max} e^{-b} \left[\sigma_j \gamma \rho + (1 - \rho)(1 - \sigma_j (1 - \gamma)) \right]}{\sigma_j \gamma} \tag{S8}$$

Density-dependent retrogression.

$$\phi = \frac{1}{\sigma_j \gamma} \left[(1 - \sigma_a) \left(1 - \sigma_j (1 - \gamma) \right) - \sigma_a \rho_{max} \ln 2 (\sigma_j - 1) \right] \tag{S9}$$

Density-dependent reproductive output.

$$\phi_{max} = e^b \left(\frac{\left[1 - \sigma_j (1 - \gamma) \right] \left[1 - \sigma_a (1 - \rho) \right]}{\sigma_j \gamma} - \sigma_a \rho \right) \tag{S10}$$

S3 Selecting virtual species

We subsetted the COMADRE Animal Matrix Database (Salguero-Gómez et al., 2016) and the COMPADRE Plant Matrix Database (Salguero-Gómez et al., 2015) to matrix population models that are ergodic, irreducible, and primitive. Doing so guarantees the existence of a single dominant eigenvalue (Caswell, 2001, pp. 83-85). We imposed a series of selection criteria on the 3,488 matrix population models available in COMADRE (v. 4.23.3.1) and 8,994 models in COMPADRE (v. 6.23.5.0) to ensure fair comparisons. The criteria are as follows: We retained only models (1) built from demographic data on *both* survival and reproduction, so complete life-cycle information was available; (2) collected in observational ("wild", *i.e.*, non-laboratory) settings without experimental manipulations so the models would reflect the dynamics of natural populations; and (3) published and digitized such that survival and reproduction are separable (*i.e.*, there are

separate **F** and **U** matrices). The latter criterion is particularly necessary here to separate the proportion of the matrix element $a_{1,2}$ that corresponds to reproductive output *vs.* to (potentially) retrogression. Finally, (5) we excluded models with clonal reproduction because permitting fair comparisons between studies with and without clonal reproduction requires careful consideration of ramet *vs.* genet dynamics (Janovský and Herben, 2020) and their emergent vital rates (Salguero-Gómez, 2018). As such, in our virtual species model, we also do not include clonal reproduction.

For each matrix population model that met our criteria, we coerced it into the same two-stage model that we are using (see Equation 1 in the main text), that is, a two stage model. When models are digitized for the databases, each stage of the model is identified as a propagule, an active member of the population, or a dormant member of the population. Based on the non-zero columns of the fertility (**F**) matrix, we can also identify each life stage as reproductive or non-reproductive. With the columns of the fertility (**F**) and survival-growth (**U**) matrices correctly identified, we can collapse the models down into a 2×2 matrix model (Salguero-Gómez and Plotkin, 2010). This last step was performed using the `mpm_collapse` function in the `Rage` package (Jones et al., 2022) in the R programming language.

We then eliminated any collapsed models with incorrect survival values (σ_j or σ_a >1). Finally, we restricted our set of observed models to those with a population growth rate (λ, the dominant eigenvalue of the projection matrix) between 1.0 and 1.6. We chose this range as a realistic comparison with our density-dependent models: at equilibrium ("carrying capacity"), our virtual species models will have $\lambda = 1$ and in early tests of the density-dependent reproductive output scenario, the highest population growth (at $N \to 0$) was $\lambda \approx 1.6$. Finally, we removed models with extremely high or extremely low reproductive output, with outliers defined as values for ϕ that fall outside of the interval $[LQ - 1.5 * IQR, UQ + 1.5 * IQR]$, where LQ is the lower quartile, UQ is the upper quartile, and IQR is the interquartile range. This final step resulted in a matrix population model for 410 animal, 872 plant, and three fungi populations, representing 100, 204, and one species, respectively (Supplemental Materials Table S4).

Supplemental References

Caswell, H. (2001). *Matrix population models* (2nd ed.). Sinauer Associates.

Janovský, Z., & Herben, T. (2020). Reaching similar goals by different means – differences in life-history strategies of clonal and non-clonal plants. *Perspectives in Plant Ecology, Evolution and Systematics*, *44*, 125534. https://doi.org/https://doi.org/10.1016/j.ppees.2020.125534

Jones, O. R., Barks, P., Stott, I., James, T. D., Levin, S., Petry, W. K., Capdevila, P., Che-Castaldo, J., Jackson, J., Römer, G., Schuette, C., Thomas, C. C., & Salguero-Gómez, R. (2022). Rcompadre and Rage—two R packages to facilitate the use of the COMPADRE and COMADRE databases and calculation of life-history traits from matrix population models. *Methods in Ecology and Evolution*, *13*(4), 770–781. https://doi.org/https://doi.org/10.1111/2041-210X.13792

Salguero-Gómez, R. (2018). Implications of clonality for ageing research. *Evolutionary Ecology*, *32*, 9–28. https://doi.org/10.1007/s10682-017-9923-2

Salguero-Gómez, R., Jones, O. R., Archer, C. R., Bein, C., de Buhr, H., Farack, C., Gottschalk, F., Hartmann, A., Henning, A., Hoppe, G., Römer, G., Ruoff, T., Sommer, V., Wille, J., Voigt, J., Zeh, S., Vieregg, D., Buckley, Y. M., Che-Castaldo, J., … Vaupel, J. W. (2016). COMADRE: A global data base of animal demography. *Journal of Animal Ecology*, *85*(2), 371–384. https://doi.org/10.1111/1365-2656.12482

Salguero-Gómez, R., Jones, O. R., Archer, C. R., Buckley, Y. M., Che-Castaldo, J., Caswell, H., Hodgson, D., Scheuerlein, A., Conde, D. A., Brinks, E., Buhr, H., Farack, C., Gottschalk, F., Hartmann, A., Henning, A., Hoppe, G., Römer, G., Runge, J., Ruoff, T., … Vaupel, J. W. (2015). The COMPADRE plant matrix database: An open online repository for plant demography. *Journal of Ecology*, *103*, 202–218. https://doi.org/10.1111/1365-2745.12334

Salguero-Gómez, R., & Plotkin, J. B. (2010). Matrix dimensions bias demographic inferences: Implications for comparative plant demography. *The American Naturalist*, *176*(6), 710–722. https://doi.org/10.1086/657044

S4 Supplemental Figures and Tables

Table S1: The contribution of each vital rate to the first two principal component axes (PC1 and PC2). Loadings in bold indicate a high contribution (greater than ±0.50) of the life-history trait to the PC axis.

Vital rate	Symbol	PC1	PC2
Juvenile survival	σ_j	**0.579**	0.269
Progression	γ	**-0.529**	-0.408
Adult survival	σ_a	**0.569**	0.123
Retrogression	ρ	0.094	0.450
Reproductive output	ϕ	-0.230	**0.735**
Proportion of variance		0.438	0.263
Cumulative proportion of variance		0.438	0.701

Table S2: The effects of vital rates and principal component axes on the resilience metrics of compensation, resistance, and recovery time in our virtual species. For each resilience metric, we fit two separate regression models. First, we fit a linear regression with strictly additive terms for each vital rate. Second, we fit a linear regression for the principal component axes including additive terms and their interaction.

Vital rate	Symbol	Regression coefficient		
		Compensation	Resistance	Recovery Time
Juvenile survival	σ_j	-0.402	0.838	-3.679
Progression	γ	-0.351	-0.085	0.588
Adult survival	σ_a	0.626	-0.076	-4.689
Retrogression	ρ	0.152	0.048	2.687
Reproductive output	ϕ	0.771	-0.036	0.201
PC axis 1		-0.094	0.135	-0.805
PC axis 2		0.604	-0.060	-0.383
Interaction PC1 and PC2		-0.023	0.002	-0.705

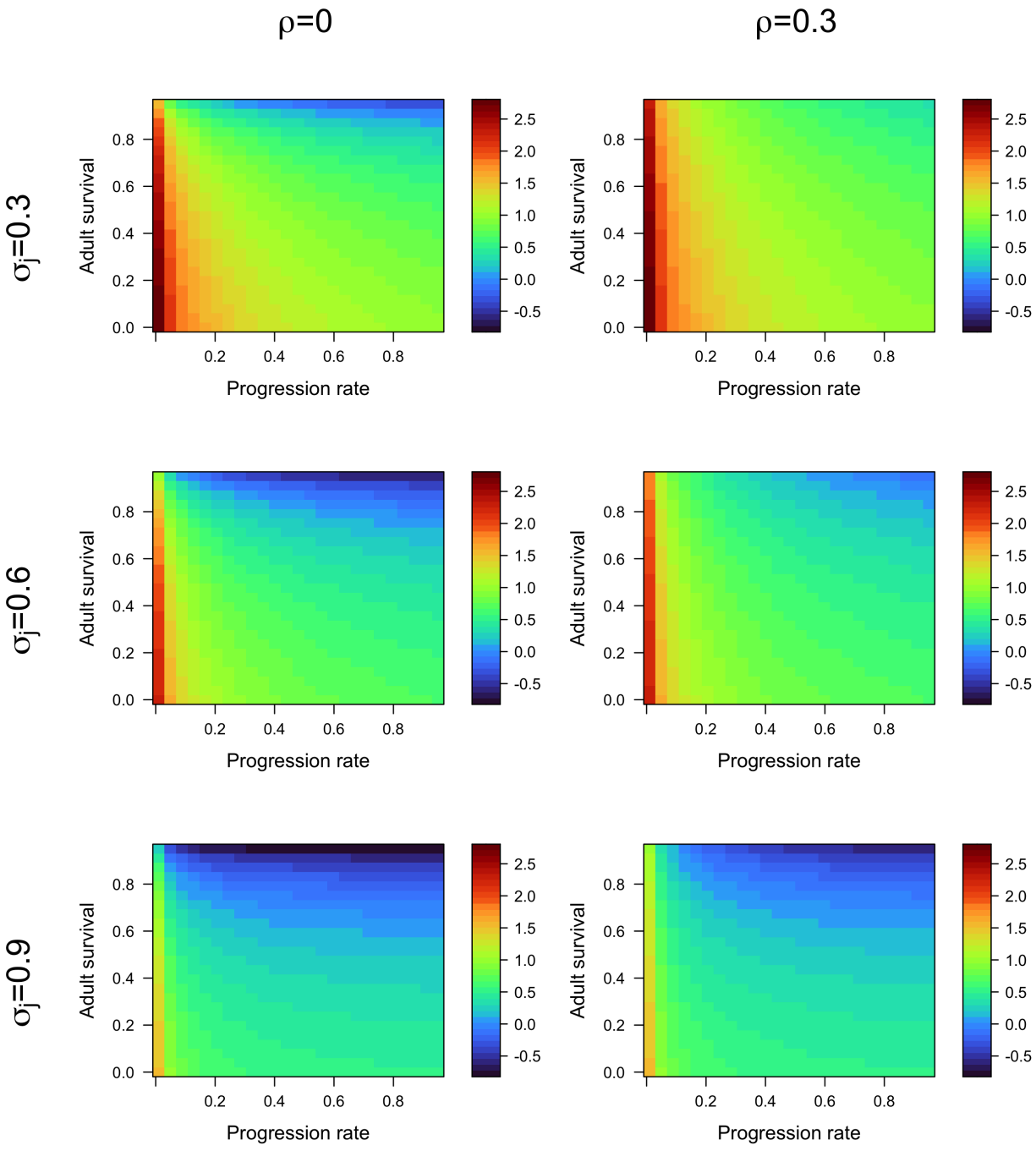

Figure S1: An example of how our model scaling affects maximum reproductive output (ϕ_{max}) across other vital rates. In this case, reproductive output is density-dependent, and the model is scaled such that the population is at its carrying capacity ($\lambda = 1$) when population density ($n_a + n_j$) is equal to 1. In each panel, we show how ϕ_{max} varies across progression (γ) and adult survival (σ_a) for a given value of juvenile survival (σ_j) and retrogression (ρ). The color scales are $\log_{10}(\phi_{max})$.

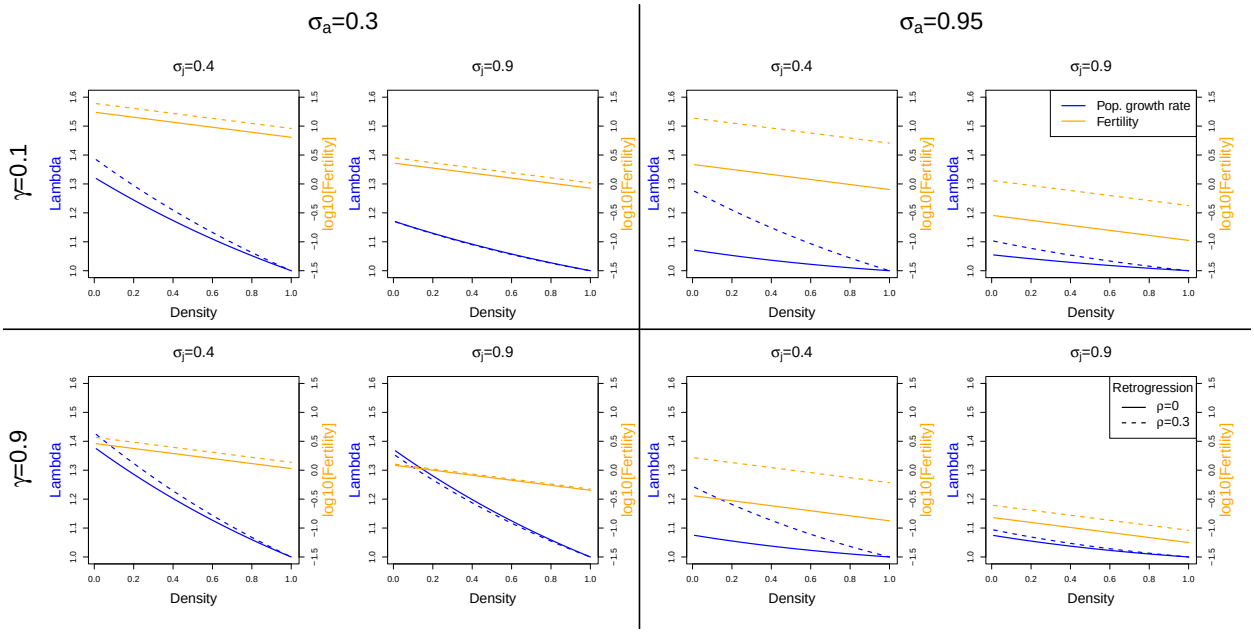

Figure S2: Population growth rate (λ) and per-capita reproductive output (ϕ) across population density for 16 virtual species models, density dependence impacts the per-capita reproductive output (ϕ).

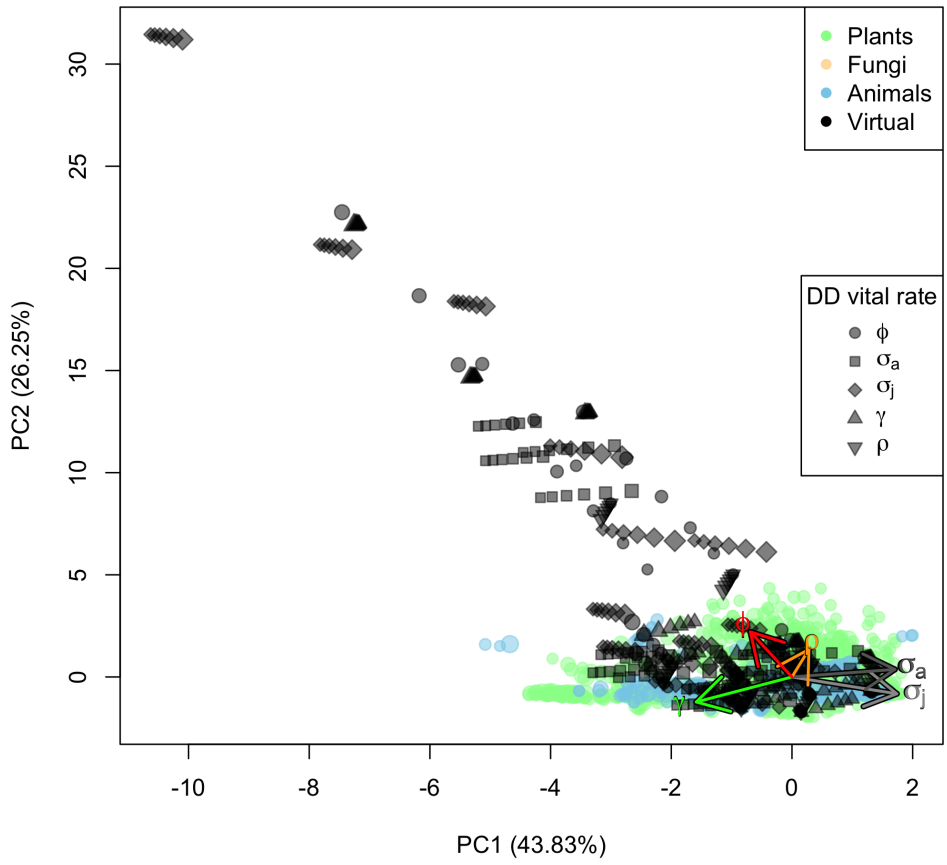

Figure S3: Some of the virtual species and density-dependent vital rate scenarios corresponded to extreme values of PC2, falling far from the space defined by empirical models. he parameters are: juvenile survival (σ_j), juvenile progression (γ), adult survival (σ_a), adult retrogression (ρ), and reproductive output (ϕ). The PCA space is defined by the observed models (colored circles, sized according to their asymptotic population growth rate, λ). The virtual species, shown in black, were then projected onto the PCA space. Each virtual species was modelled with density dependence on each of the five vital rates (shown with different shapes), and each density-dependent scenario was plotted for six values of density between 0 and 1, sized according to λ.

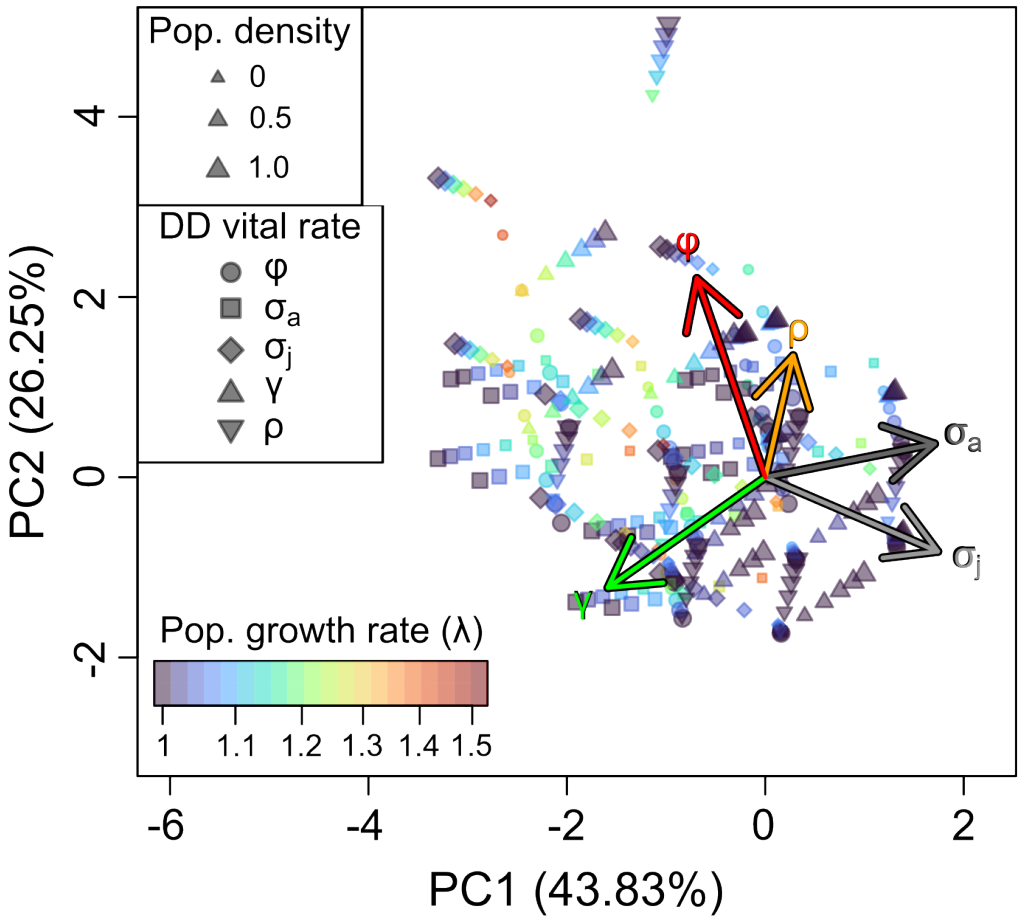

Figure S4: Population growth rate in virtual species models changes across life history strategies and density-dependent scenarios. The vital rates are: juvenile survival (σ_j), adult survival (σ_a), juvenile progression (γ), adult retrogression (ρ), and reproductive output (ϕ). The principal component (PC) axes were defined using empirical models of 1,285 natural/wild populations of animals and plants (see Fig. S3). The virtual species have then been projected onto the PC axes. Each virtual species was modeled with density dependence on each of the five vital rates. For each density-dependent scenario, the virtual species model was calculated for six values of density between 0 and 1 (plot symbols sized according to population density).

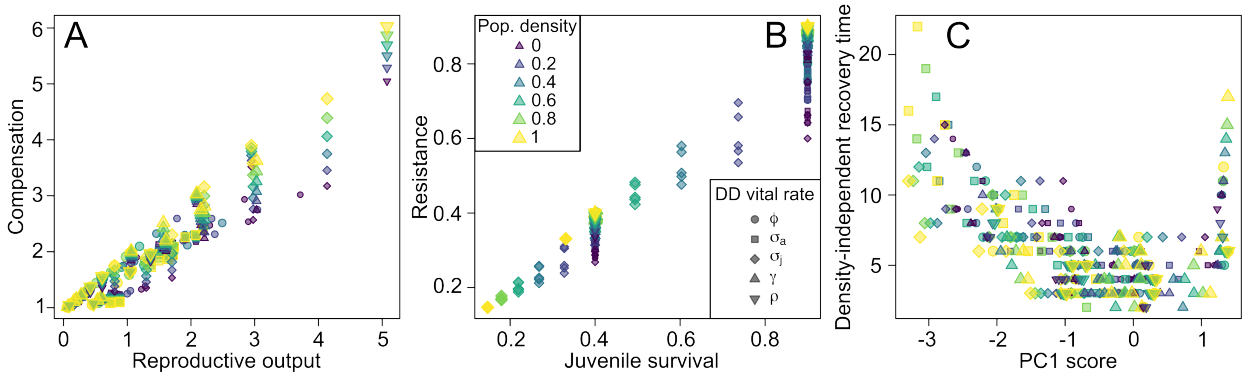

Figure S5: Resilience metrics for our virtual species show strong relationships with demographic rates. The demographic rates with the strongest relationships to the resilience metrics were (A) reproductive output for compensation and (B) juvenile survival for resistance. Density-independent recovery time showed a complicated and non-linear relationship with demographic rates, and density-independent recovery times were longest for virtual species with extreme scores on PC1.

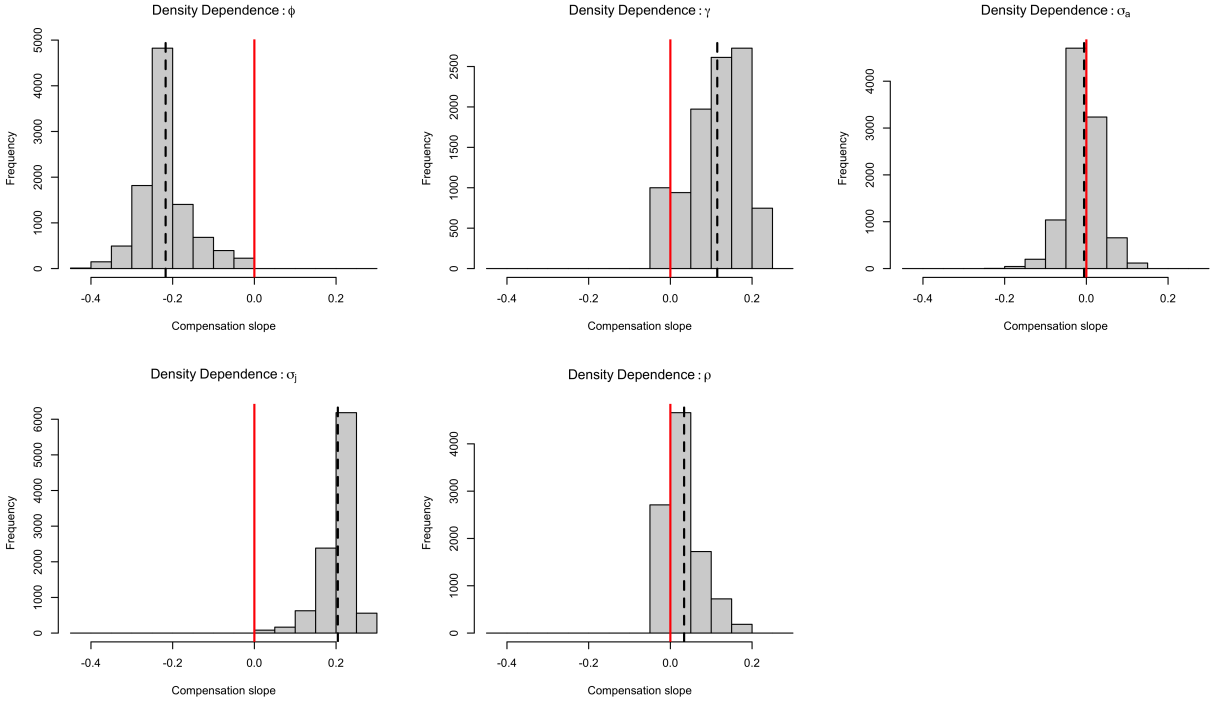

Figure S6: The distribution of compensation slope values depends on which vital rate is the target of density dependence. For each density dependence scenario, we calculated the slope of compensation across densities (*i.e.*, a in $\log_{10}(C) = a * N + b$, where N is population density and C is the compensation of the population projection matrix calculated at each value of N) for the full range of possible vital rates: $\sigma_j \in [0.01, 1]$; $\gamma \in [0.01, 0.95]$; $\sigma_a \in [0, 0.95]$; and $\rho \in [0, 1]$. For each vital rate, we calculated slopes at 10 values, yielding a total of 10^4 vital rate combinations for each density dependence scenario. In each panel, a slope of 0 is highlighted with a solid red line, and the mean value of slopes across all tested vital rate combinations is shown with a thick vertical dashed line.

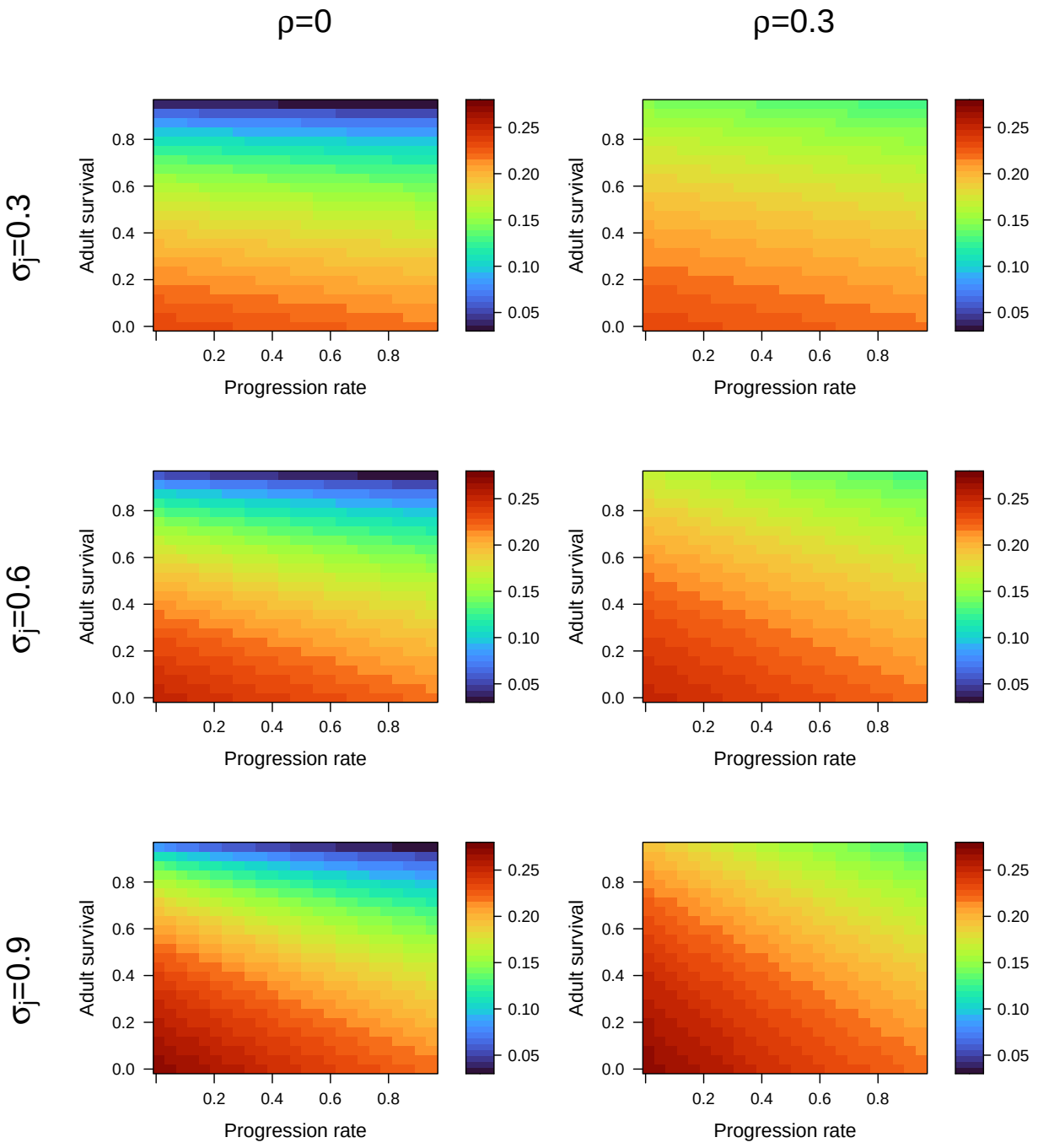

Figure S7: Strength of density effects on compensation when juvenile survival is density-dependent. We calculated the slope of compensation across population densities ($\log C \sim N_t$) for many possible parameter combinations across: $\sigma_a \in [0, 0.95]$, $\gamma \in [0.01, 0.95]$, $\sigma_j = 0.3, 0.6, 0.9$, and $\rho = 0, 0.3$. A single color scale is used for all panels. Slow life histories are in the upper left of each panel, and fast life histories are in the lower right.

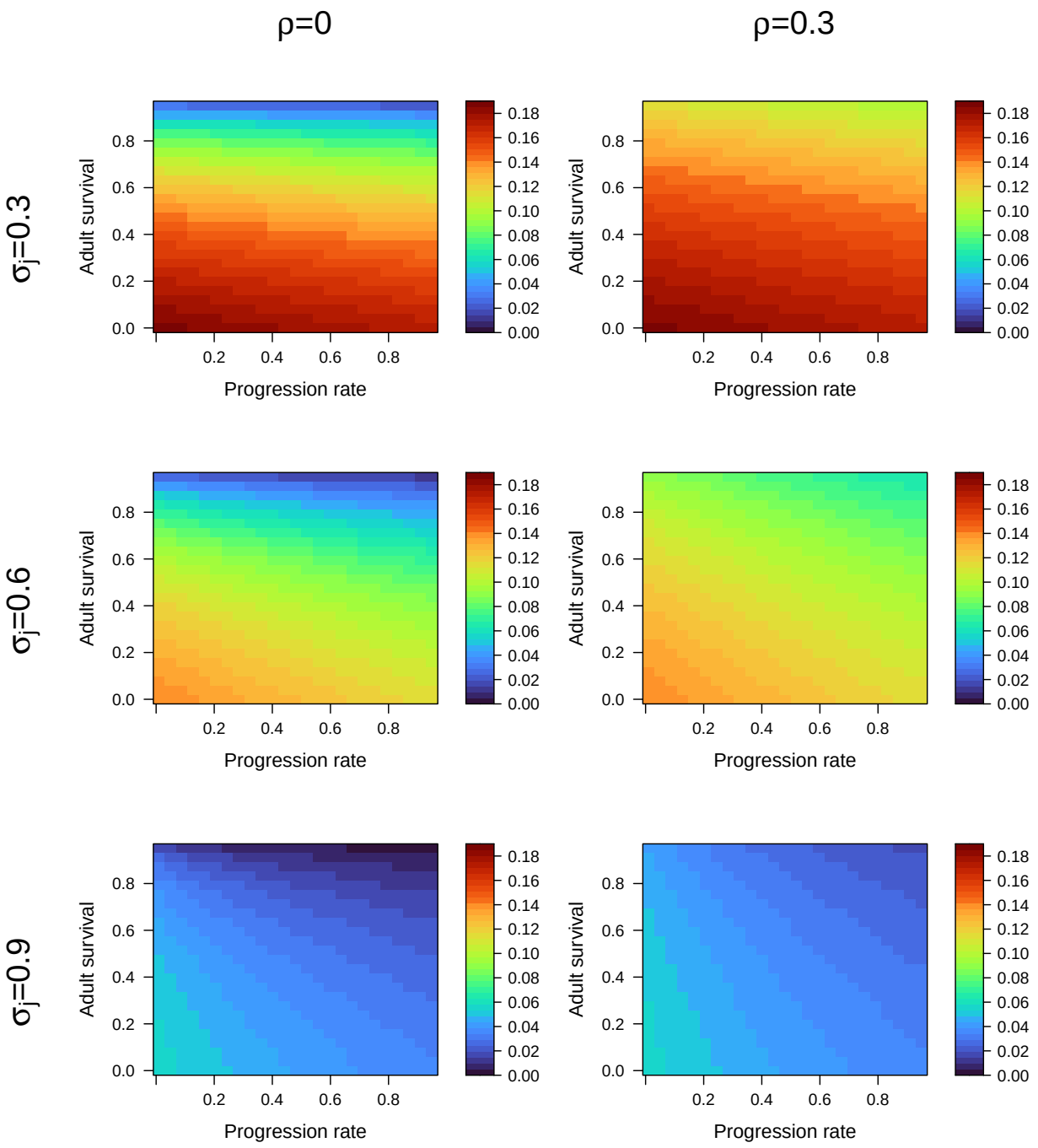

Figure S8: Strength of density effects on compensation when juvenile progression rate is density-dependent. Details are the same as Figure S7.

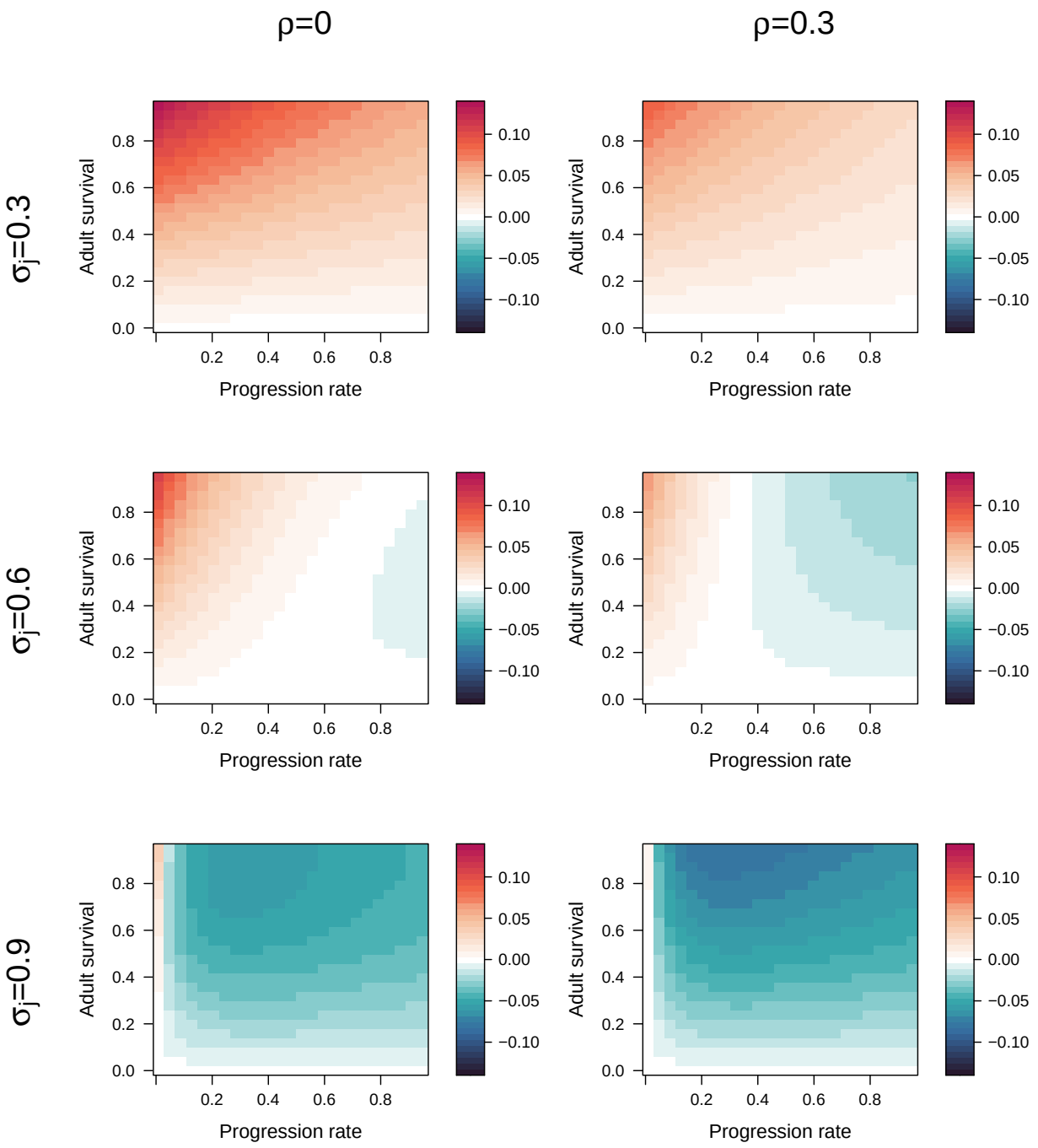

Figure S9: Strength of density effects on compensation when adult survival is density-dependent. Details are the same as Figure S7.

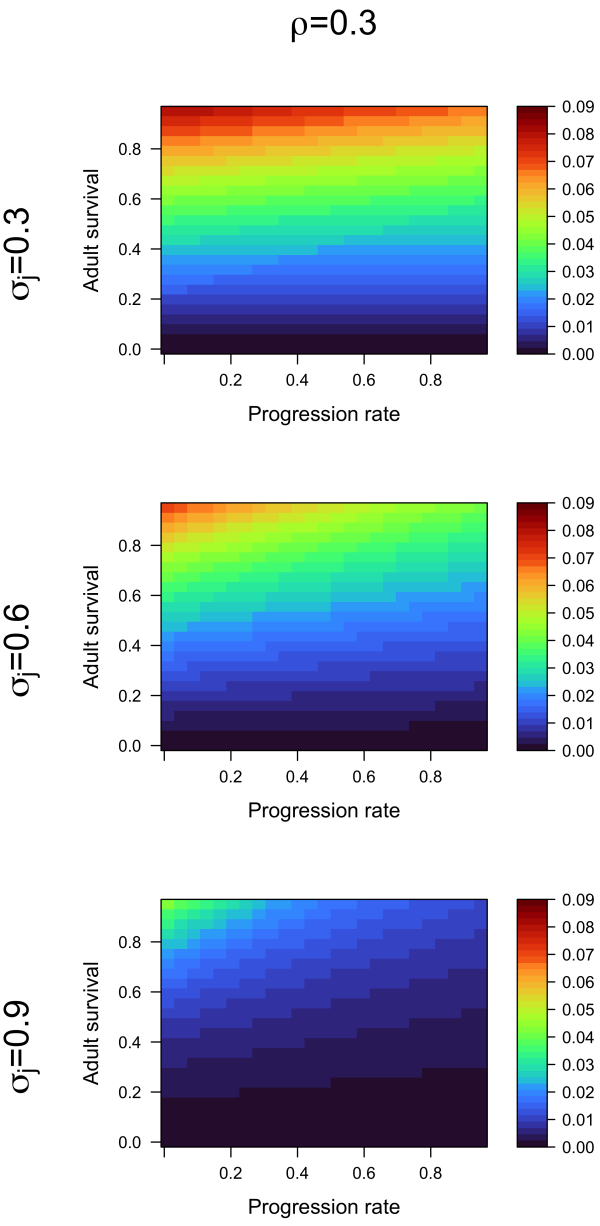

Figure S10: Strength of density effects on compensation when retrogression rate is density-dependent. Details are the same as Figure S7.

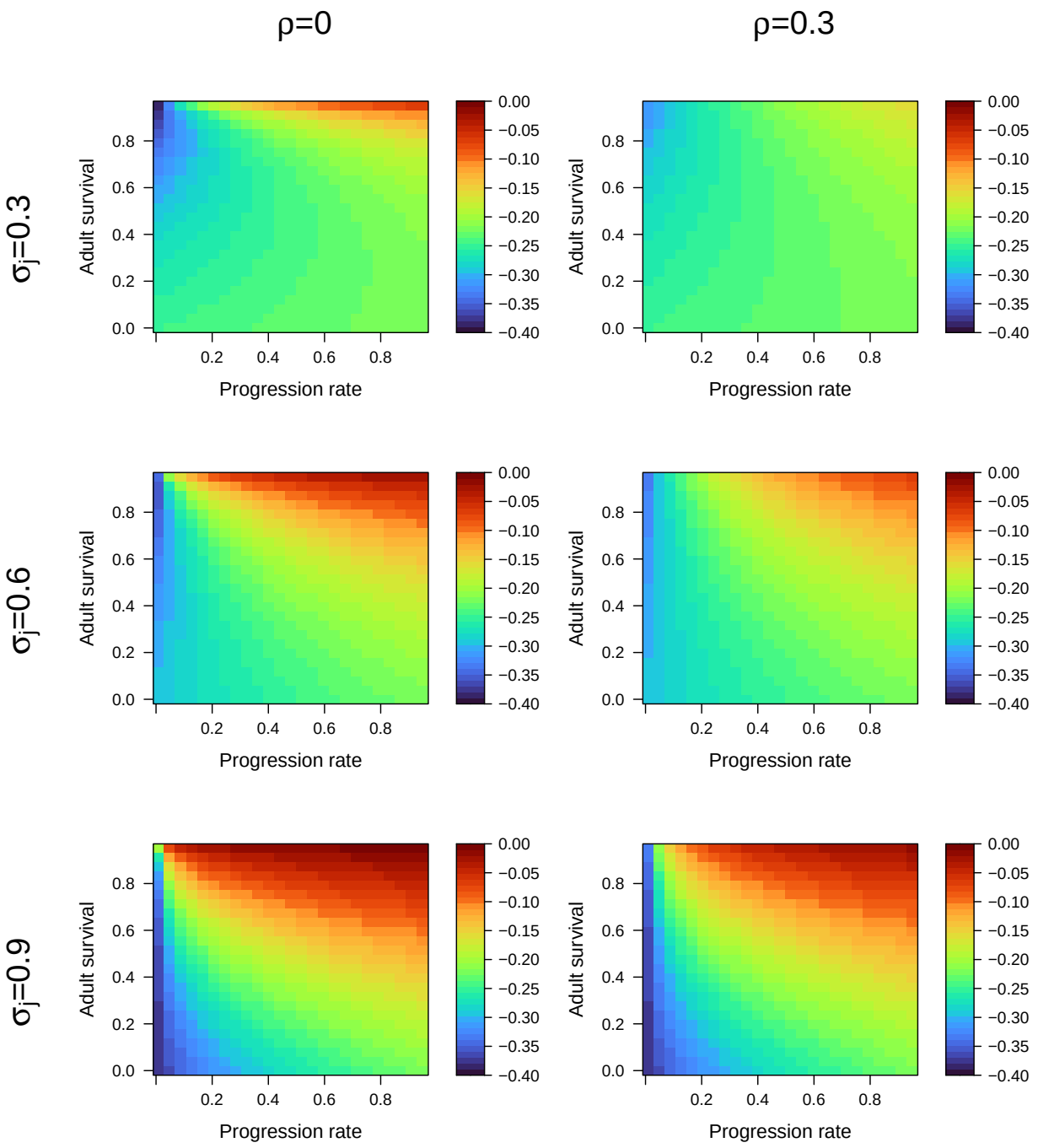

Figure S11: Strength of density effects on compensation when reproductive output is density-dependent. Details are the same as Figure S7.

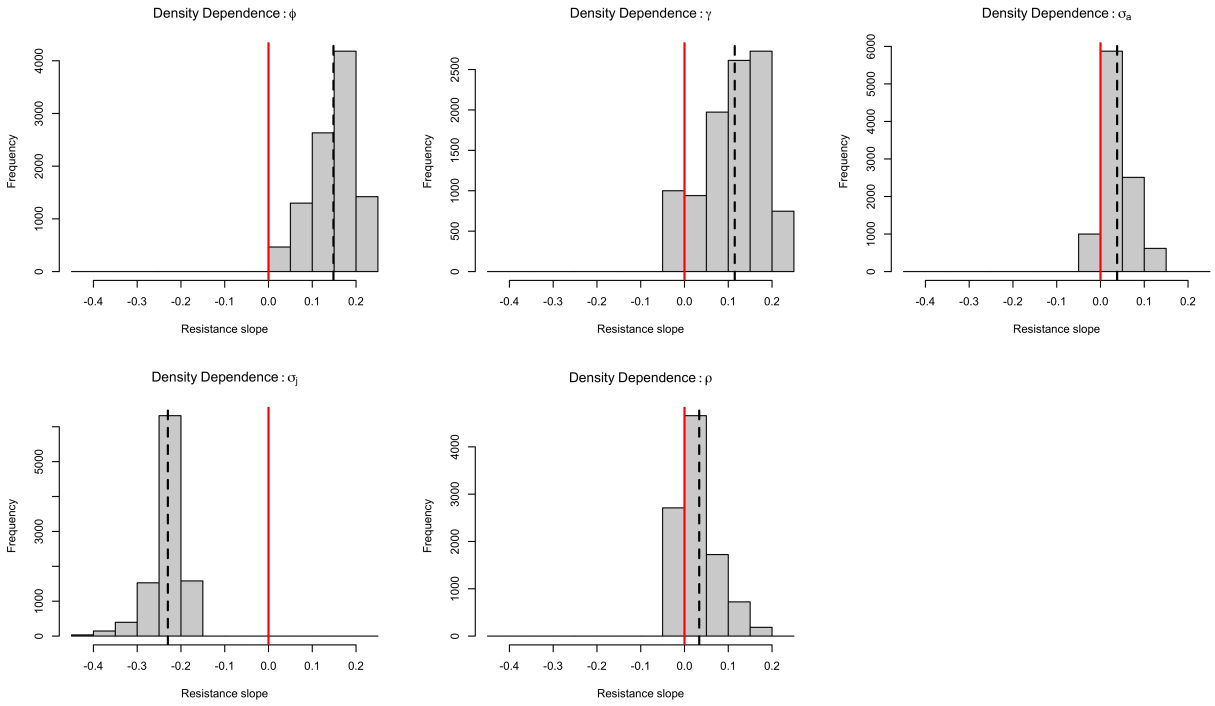

Figure S12: The distribution of resistance slope values depends on which vital rate is the target of density dependence. Details are the same as in Figure S6.

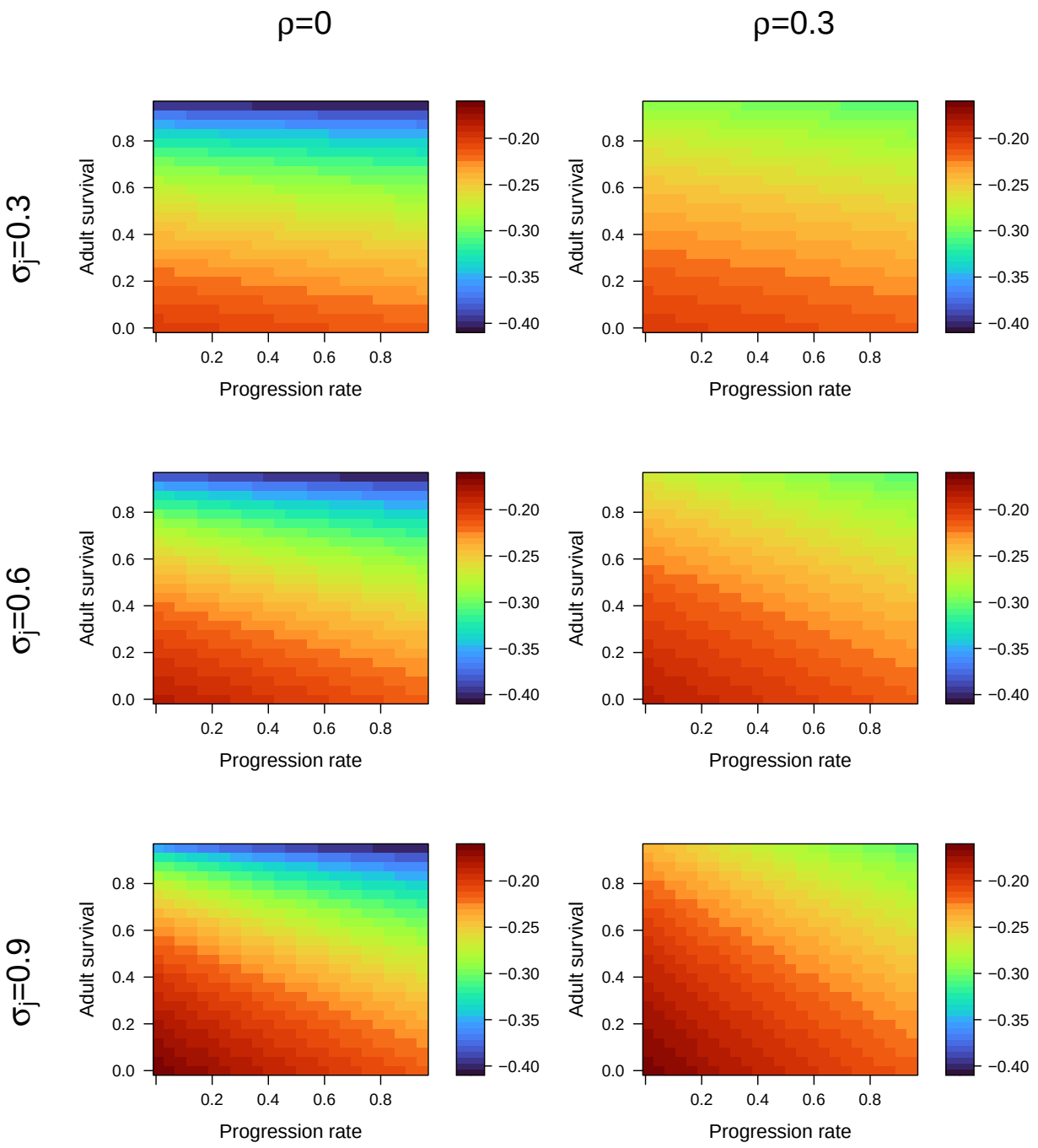

Figure S13: Strength of density effects on resistance when juvenile survival is density-dependent. Details are the same as Figure S7.

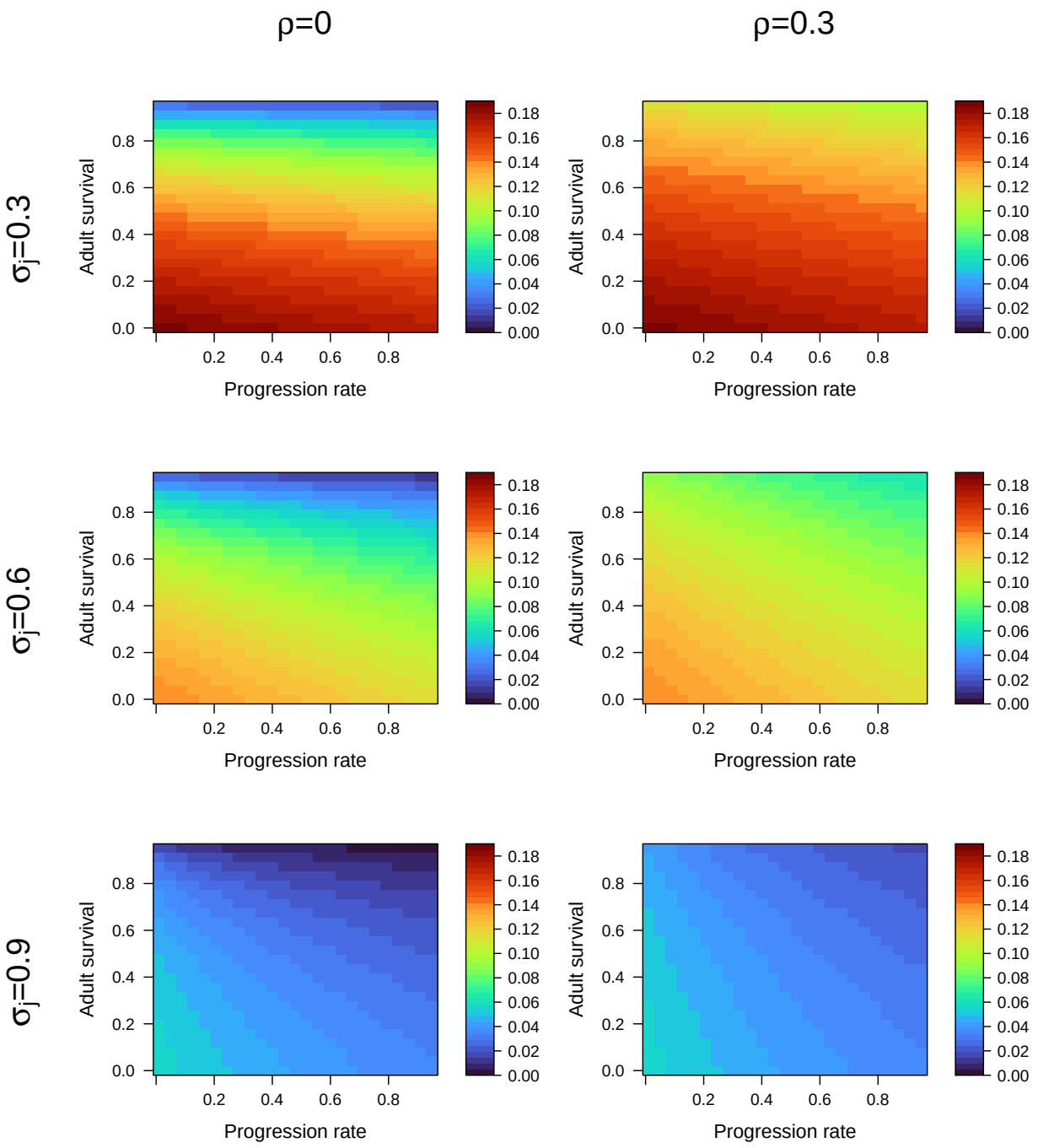

Figure S14: Strength of density effects on resistance when juvenile progression rate is density-dependent. Details are the same as Figure S7.

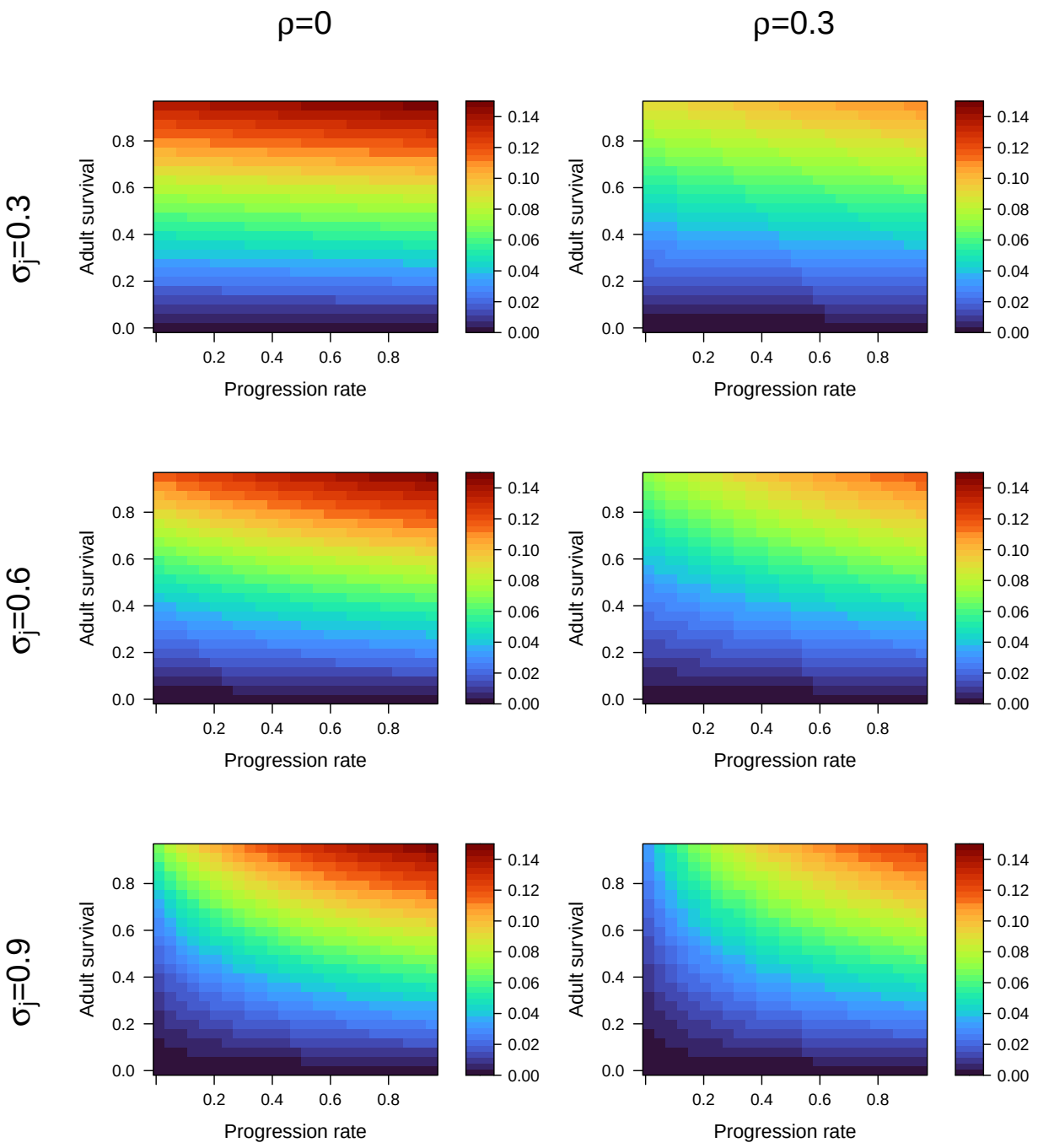

Figure S15: Strength of density effects on resistance when adult survival is density-dependent. Details are the same as Figure S7.

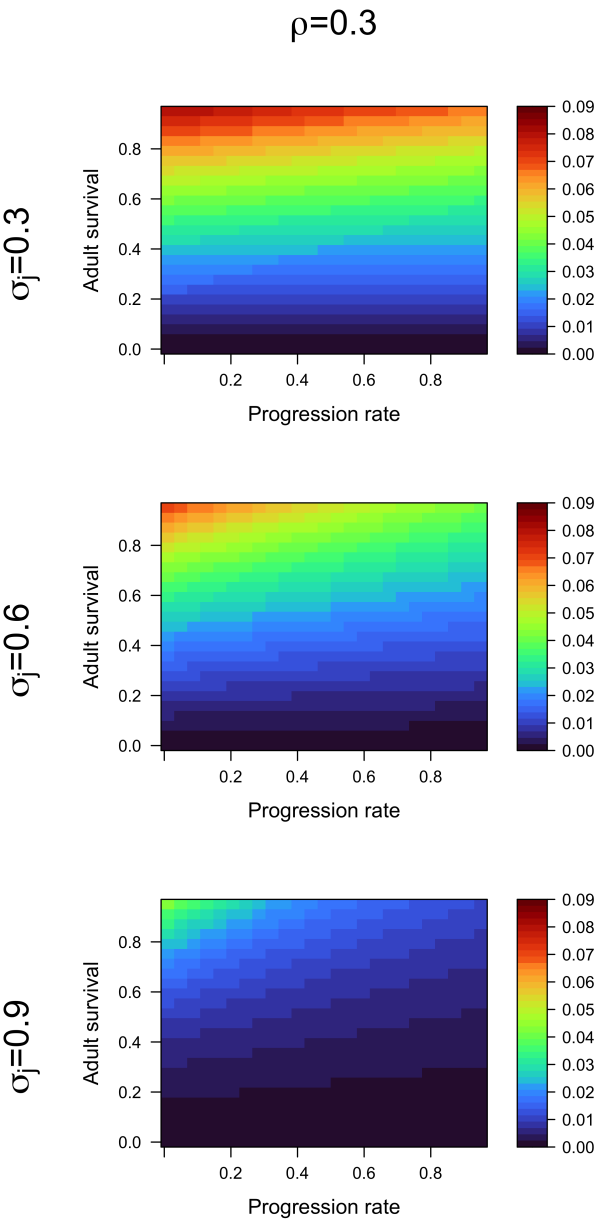

Figure S16: Strength of density effects on resistance when retrogression rate is density-dependent. Details are the same as Figure S7.

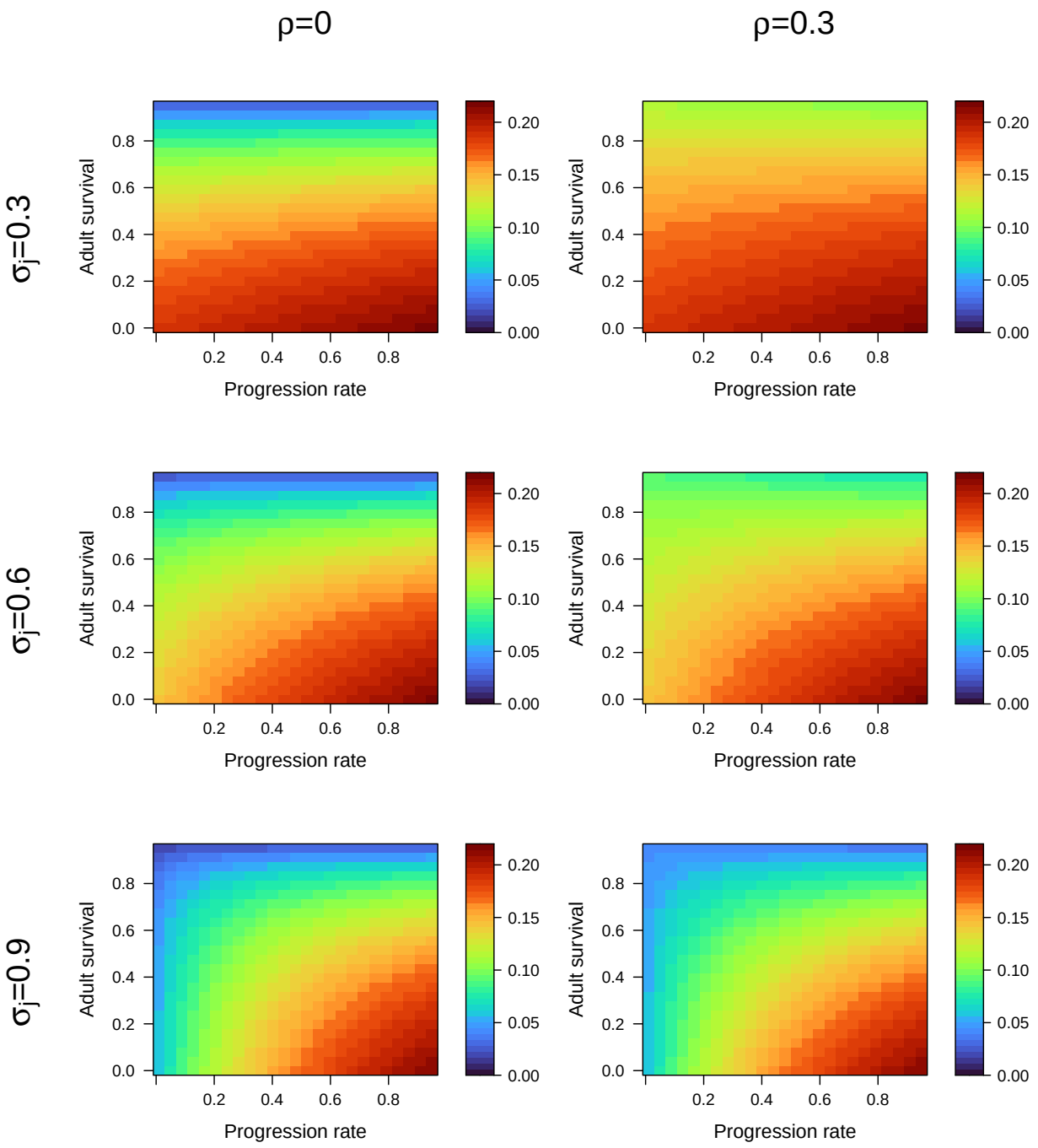

Figure S17: Strength of density effects on resistance when reproductive output is density-dependent. Details are the same as Figure S7.

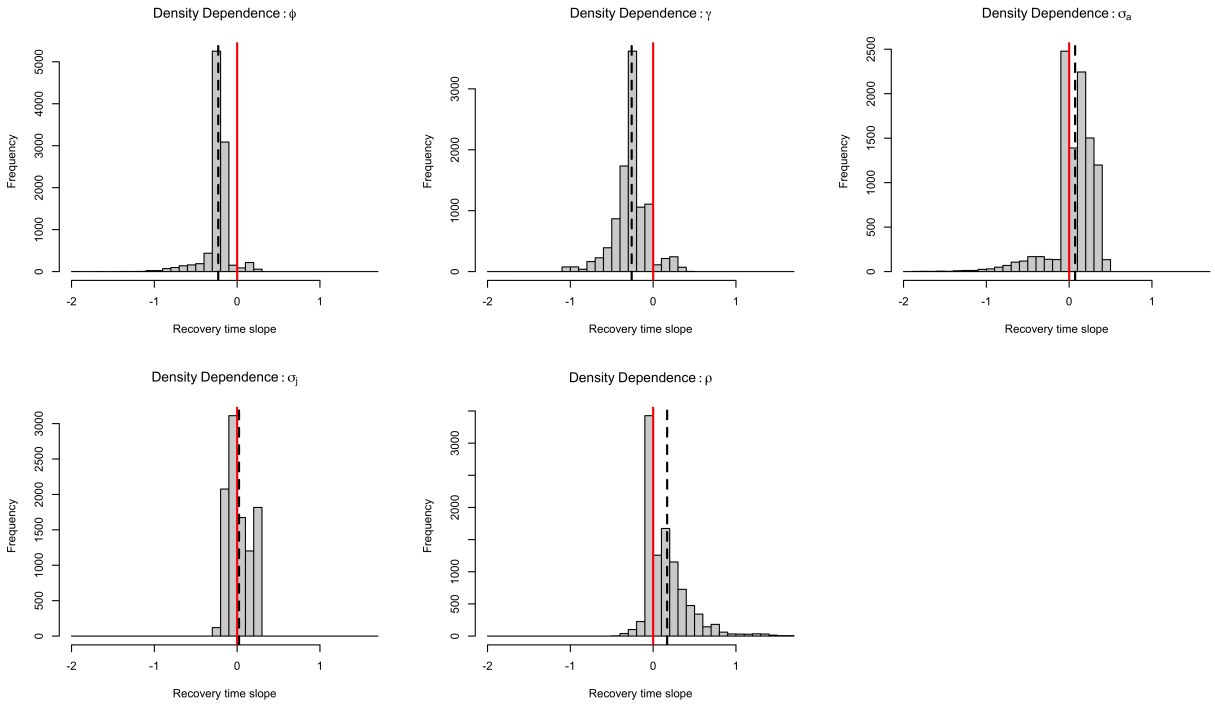

Figure S18: The distribution of density-independent recovery time slope values depends on which vital rate is the target of density dependence. Details are the same as in Figure S6.

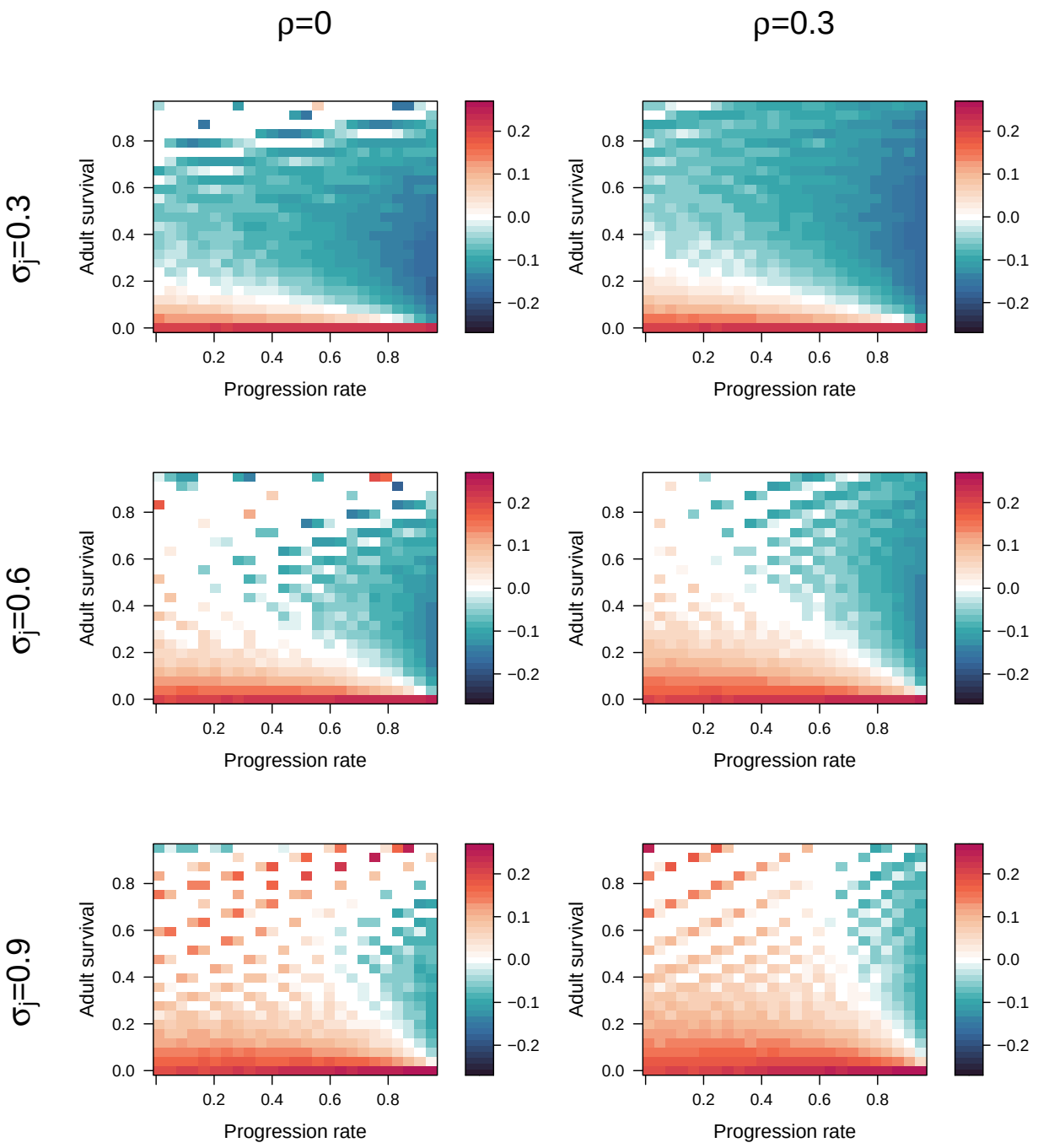

Figure S19: Strength of density effects on density-independent recovery time when juvenile survival is density-dependent. Details are the same as Figure S7.

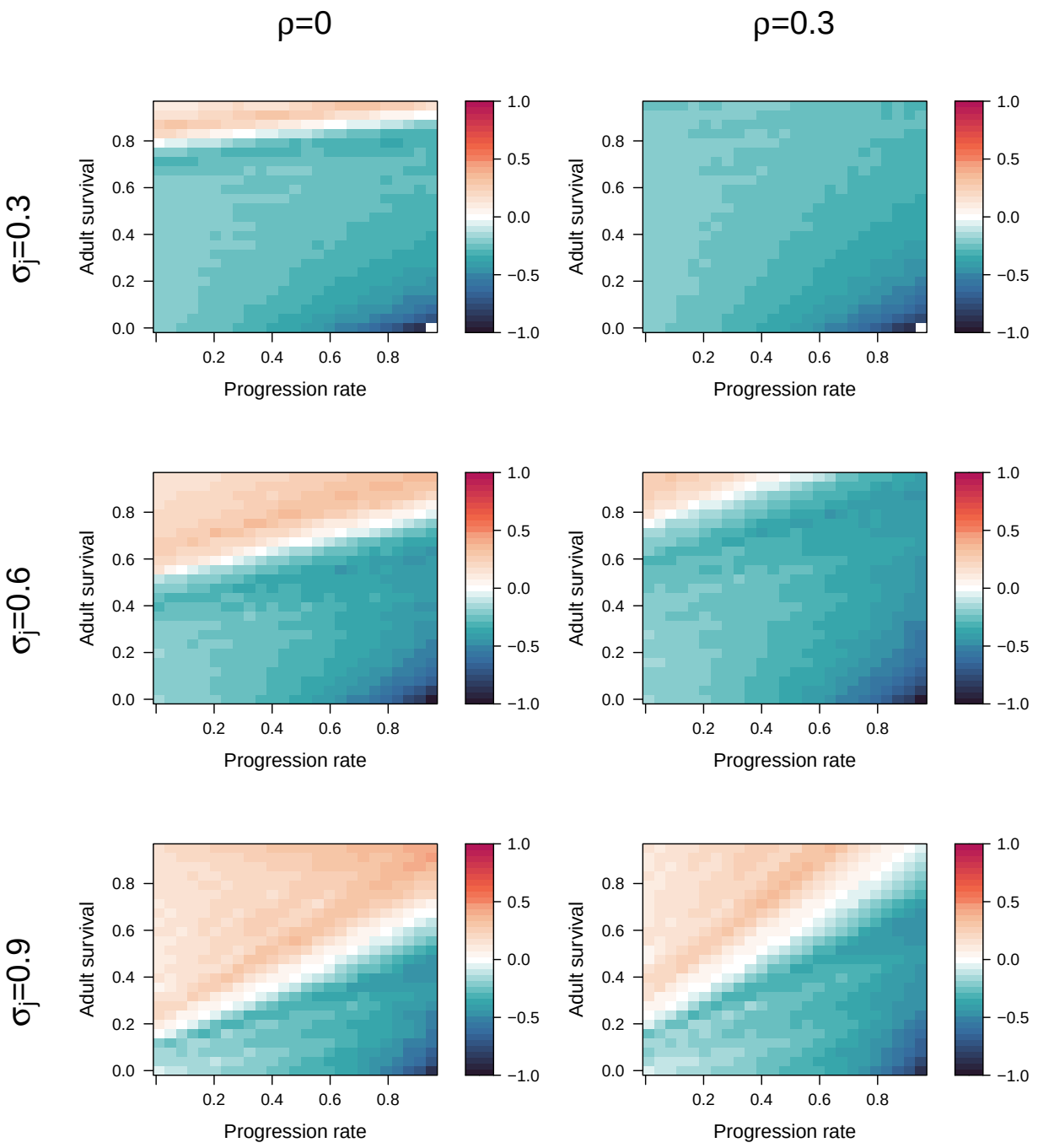

Figure S20: Strength of density effects on density-independent recovery time when juvenile progression rate is density-dependent. Details are the same as Figure S7.

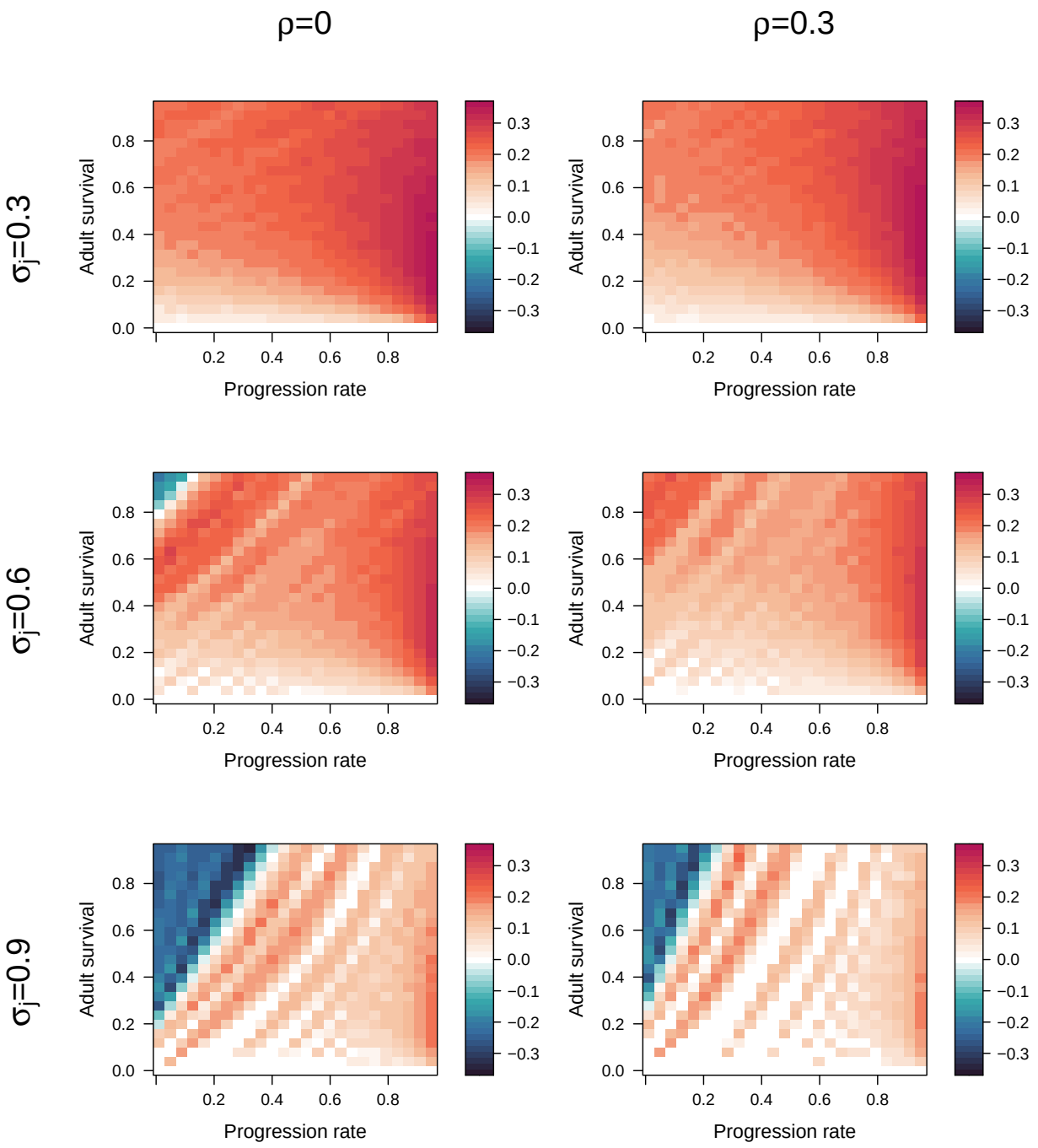

Figure S21: Strength of density effects on density-independent recovery time when adult survival is density-dependent. Details are the same as Figure S7.

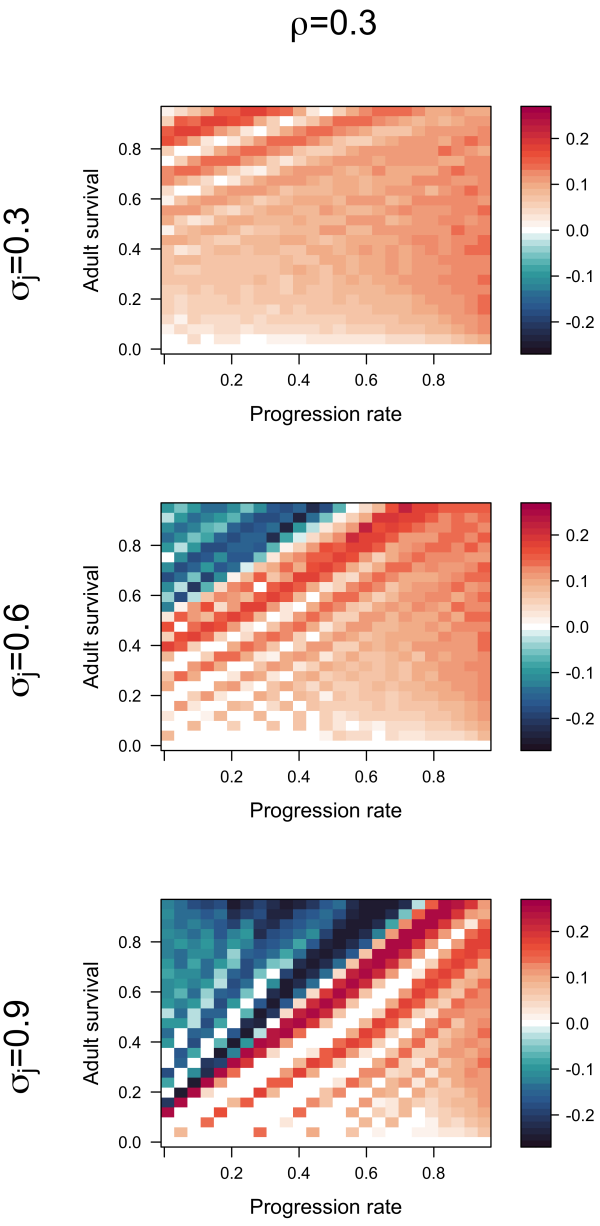

Figure S22: Strength of density effects on density-independent recovery time when retrogression rate is density-dependent. Details are the same as Figure S7.

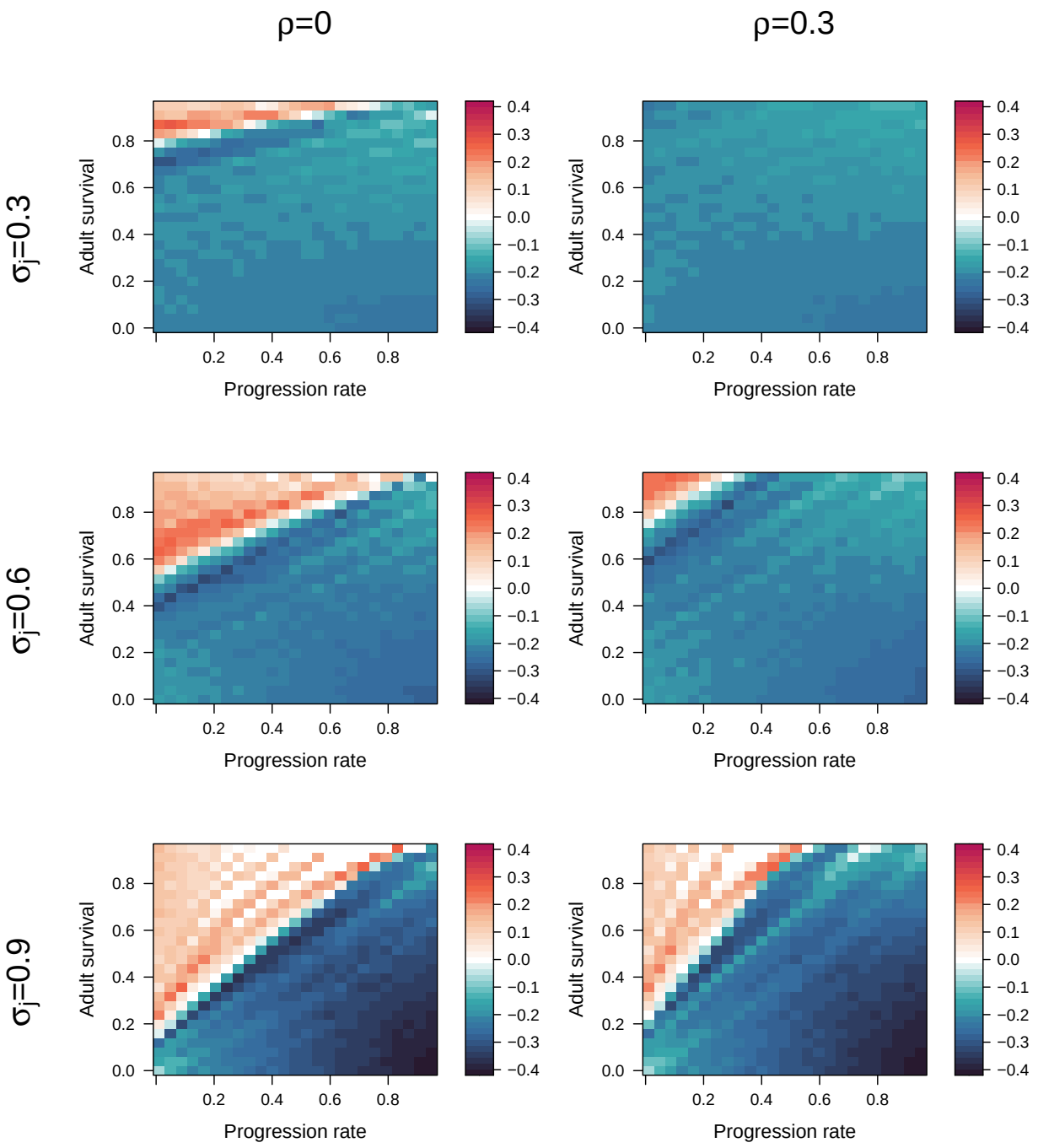

Figure S23: Strength of density effects on density-independent recovery time when reproductive output is density-dependent. Details are the same as Figure S7.

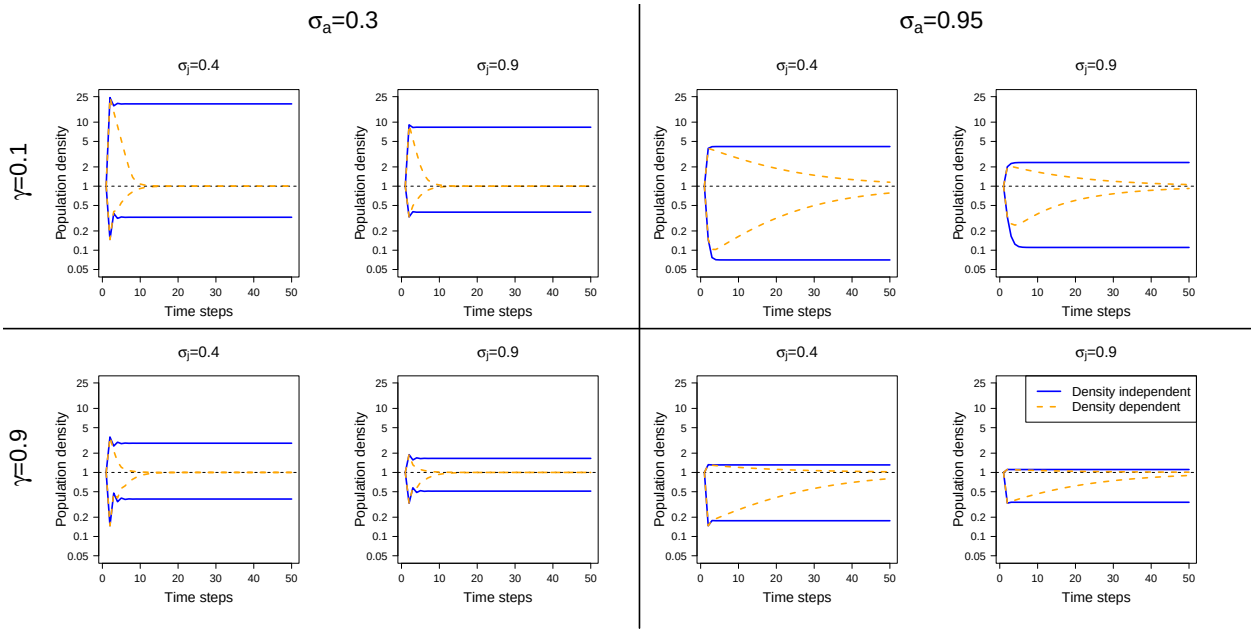

Figure S24: Variation in transient envelope patterns across our set of virtual species and between density-dependent and density-independent models. In this scenario, density dependence operates on juvenile survival (σ_j).

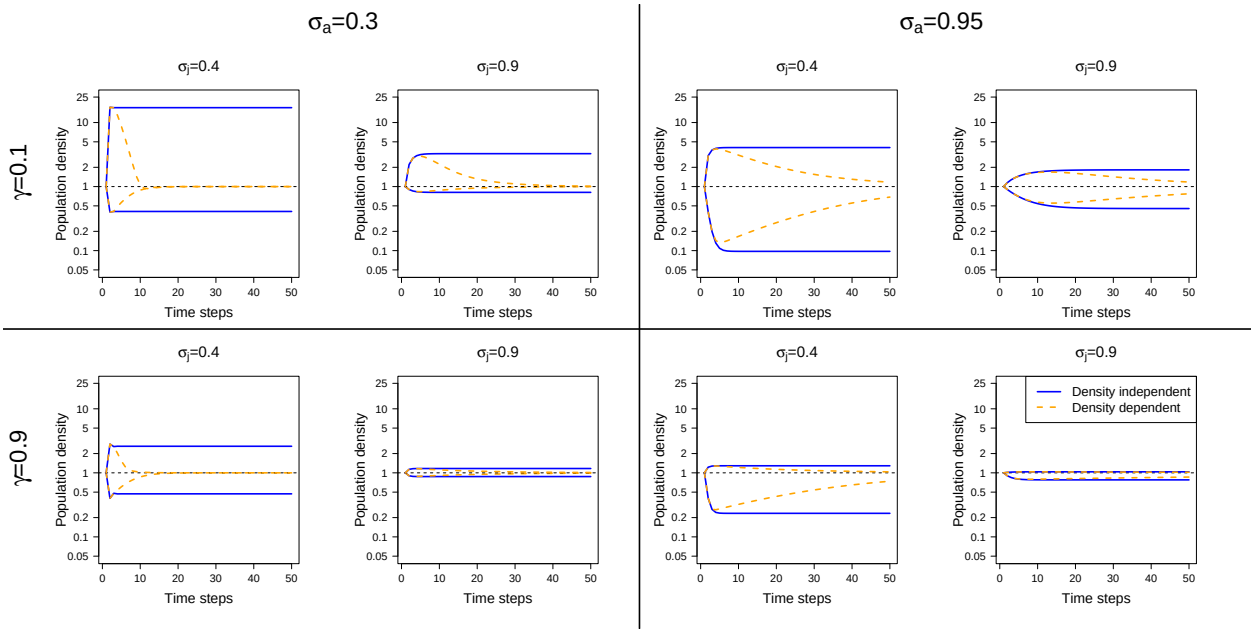

Figure S25: Variation in transient envelope patterns across our set of virtual species and between density-dependent and density-independent models. In this scenario, density dependence operates on progression rate (γ).

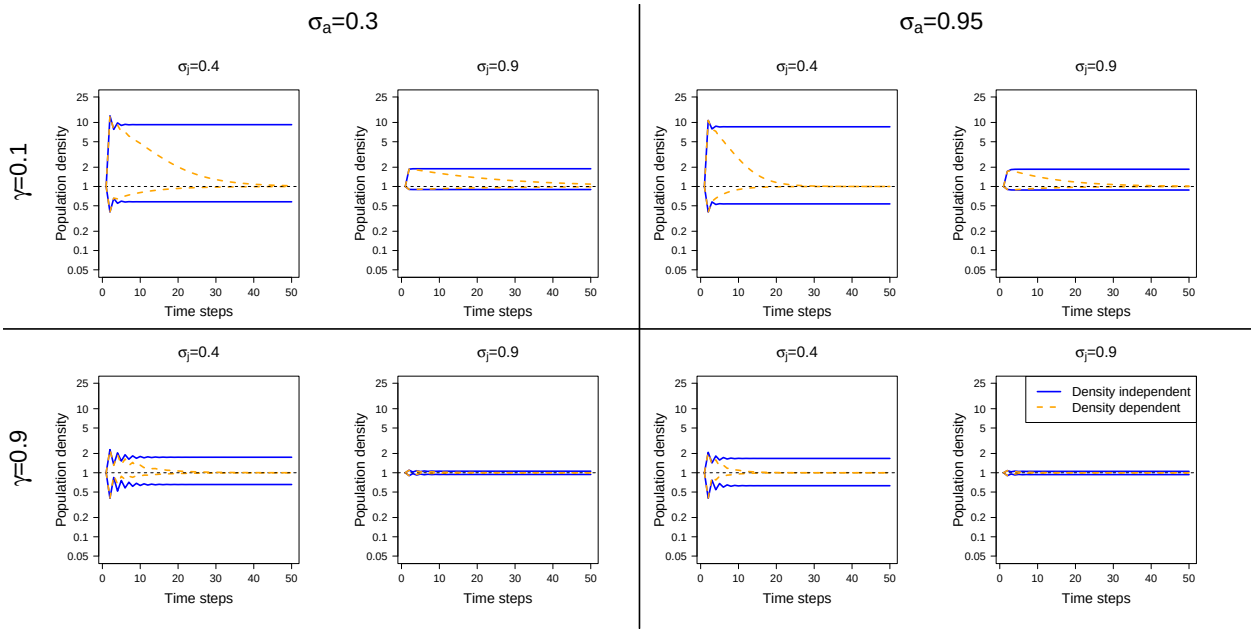

Figure S26: Variation in transient envelope patterns across our set of virtual species and between density-dependent and density-independent models. In this scenario, density dependence operates on adult survival (σ_a).

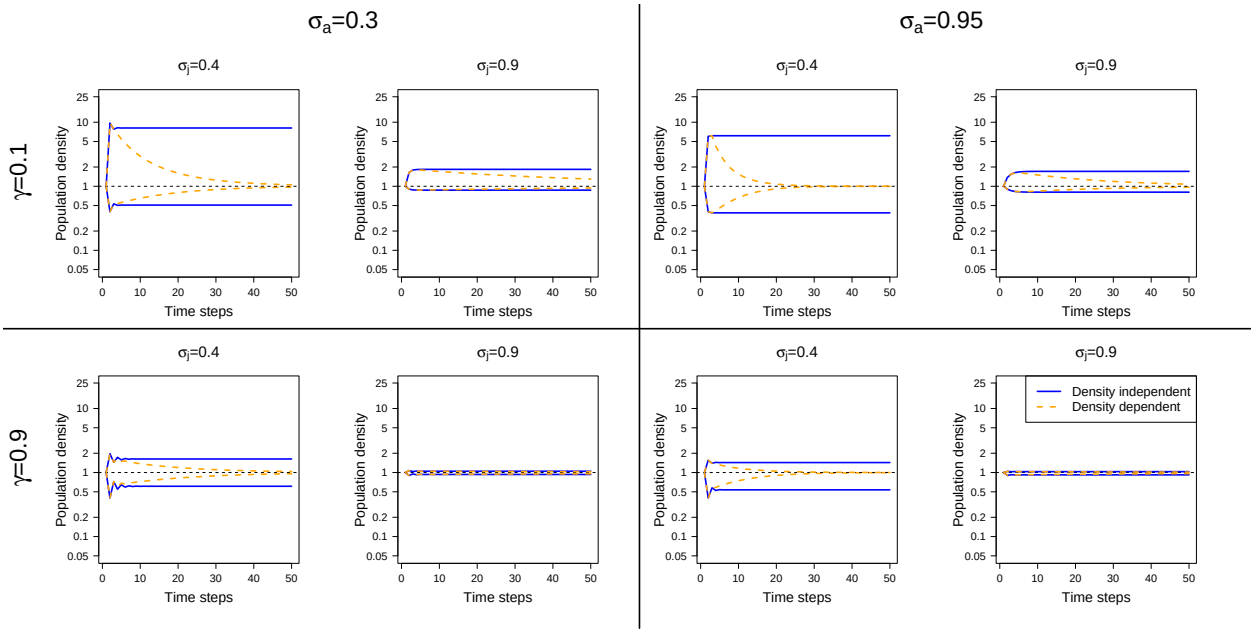

Figure S27: Variation in transient envelope patterns across our set of virtual species and between density-dependent and density-independent models. In this scenario, density dependence operates on retrogression rate (ρ).

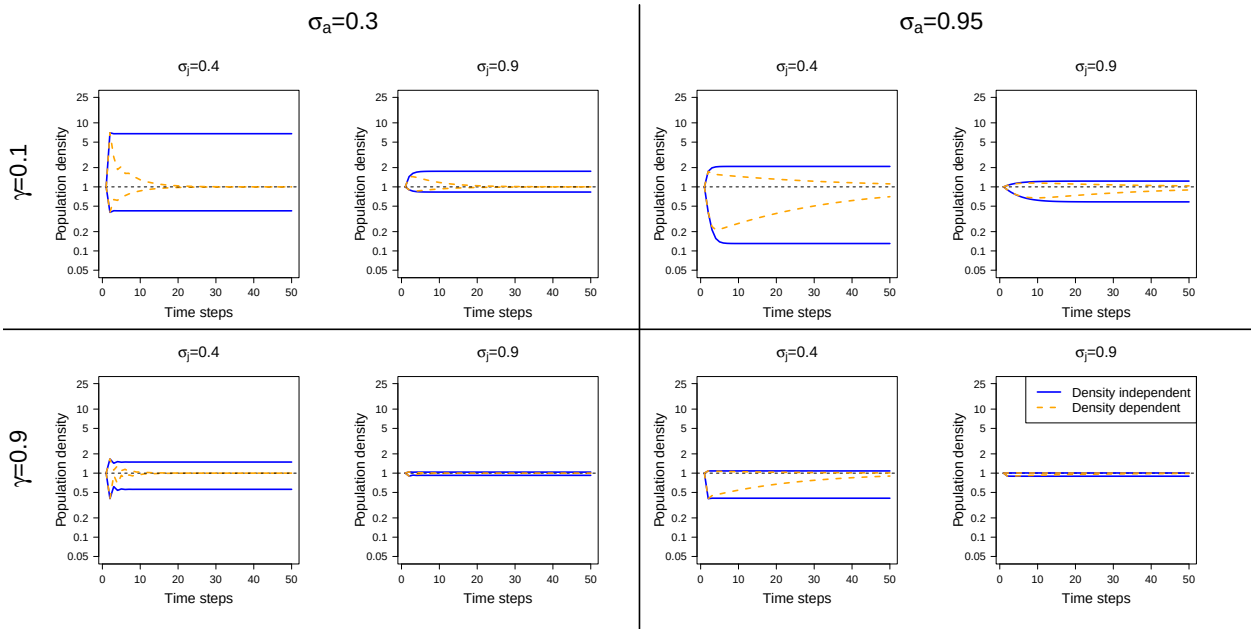

Figure S28: Variation in transient envelope patterns across our set of virtual species and between density-dependent and density-independent models. In this scenario, density dependence operates on reproductive output (ϕ).

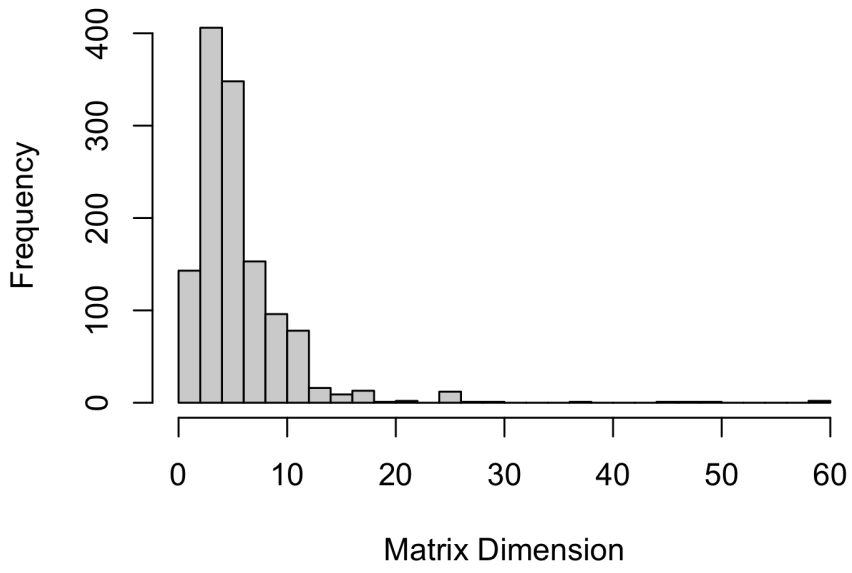

Figure S29: The matrix dimensions for empirical models used in selecting virtual species models. The matrix dimension is the number of classes included in the projection matrix. Before collapsing all the models to 2×2, most of the models were larger, representing more complex life cycles than represented by our two-stage model (Supplemental Materials Table S4).